Task-Agnostic Assistance via Centroidal Momentum Shaping: Preliminary Validations on a Hip Exoskeleton

Miao Yu[1], *Student Member, IEEE*, Jesse Dean[2], and Ge Lv[1], *Member, IEEE*

Abstract*—Model-based control paradigms for lower-limb exoskeletons may encounter challenges in securing solutions for high-dimensional, underactuated human-exoskeleton systems and often rely on task-specific reference kinematics that restrict voluntary motion. Recent learning-based methods can accommodate voluntary motion but typically require extensive data for training, and their ability to generalize beyond the training tasks remains unclear. In this paper, we propose a novel control paradigm that regulates an individual's Centroidal Momentum, *i.e.*, the sum of projected limb momenta onto the Center of Mass, by tracking a virtual reference model's Centroidal Momentum to provide task-agnostic assistance. The reference model is defined from each user's real-time gaits with scaled limb inertial parameters, rather than pre-defined reference kinematics. To accommodate voluntary motion, we propose a nonlinear disturbance observer to estimate human joint torques and incorporate it into the control design. We provide proofs for ultimate boundedness of the observer's estimation error and the closed-loop Centroidal Momentum tracking error with an exponentially decaying transient. Preliminary experiments with six non-disabled participants wearing a bilateral hip exoskeleton demonstrate the effectiveness of the proposed approach across treadmill walking, ground-stair transitions, and sit-to-stand tasks. Ensemble-averaged muscle efforts showed an average 22% reduction with assistance and a 21% increase with resistance, indicating the potential of the proposed control paradigm for task-agnostic assistance.

***Index Terms*—Prosthetics and exoskeletons, wearable robotics, optimization and optimal control.**

I. INTRODUCTION

EMERGING powered lower-limb exoskeletons have shown great potential in assisting human locomotion across diverse activities [1], such as load carriage [2], metabolic cost reduction [3], and restoration of normative gait patterns [4]. Exoskeleton control paradigms can be broadly grouped into reference kinematics-based and reference kinematics-free approaches [1]. Reference kinematics-based methods track pre-defined torque profiles [5] or enforce joint trajectories [1] via torque controllers. While this strategy is simple and accurate [6], it can constrain voluntary motion and reduce interaction friendliness [7]. In addition, many such controllers are task-specific (e.g., sit-to-stand [8] and stair climbing [9]), requiring reliable transition detection for daily use [10]. By contrast, reference kinematics-free, task-agnostic approaches do not prescribe fixed gait patterns and are better suited to assist voluntary motion across locomotor tasks.

Recent task-agnostic control studies have explored intent-driven and model-based strategies. Human-in-the-loop methods adapt assistance using user responses (e.g., metabolic cost, EMG, and gait metrics) [11]. Their main limitation lies in practicality, e.g., lengthy user-specific tuning and repeated evaluations, and the resulting parameters may transfer poorly across users, sessions, and daily tasks. Alternatively, predictive control schemes infer future gait patterns from sensory feedback such as plantar forces [12] to generate adaptive assistance that minimizes reliance on reference kinematics. However, these methods rely critically on prediction accuracy and are vulnerable to model mismatch [6]. Learning-based approaches further relax kinematic constraints by directly estimating and compensating for biological joint torques [13], but typically require large datasets for training [14] and may not generalize well to continuously varying tasks.

Task-agnostic control has also been achieved through energetic approaches. Energy shaping [15] provides consistent assistance across tasks by reducing users' perceived body weight. Notably, Lin *et al.* developed a velocity-dependent, task-agnostic controller through shaping the Hamiltonian dynamics into a desired form [16] and further improved the control performance for varying tasks via a modular, data-driven optimization framework [17]. Despite promising outcomes, these approaches require solving matching conditions, a set of nonlinear partial differential equations that determine the feasible form of closed-loop dynamics, which remains challenging for high-dimensional systems with varying degrees of underactuation, especially with limited computational capability of wearable hardware. A key open challenge is the development of a task-agnostic control paradigm that is both computationally tractable and adaptable to voluntary human motion in diverse locomotion scenarios.

Centroidal Momentum (CM), defined as the sum of the projected segmental momenta onto a rigid body's Center of Mass (CoM) [18], provides a compact, fixed-dimensional representation of whole-body dynamics. CM has been widely used in locomotion analysis and control for bipeds, with its normalized anteroposterior linear and mediolateral angular components shown to correlate strongly with balance performance during walking [19]. The fact that CM is fixed-dimensional in 3D space and remains well-defined across gait patterns and tasks makes it a natural candidate to alter to achieve task-agnostic control. As long as the available exoskeleton actuators exceed the CM's dimensionality in all three planes, a control law can be obtained to regulate all components of an individual's CM, even in underactuated systems. These properties demonstrate

Manuscript received: December 22, 2025; Revised March 27, 2026; Accepted May 14, 2026. This paper was recommended for publication by Editor Haoyong Yu upon evaluation of the Associate Editor and Reviewers' comments. The work of M. Yu and G. Lv was supported by the National Science Foundation under Award 2340261.

[1] M. Yu and G. Lv are with the Department of Mechanical Engineering, Clemson University, Clemson, SC 29634, USA. {`myu2, glv`}`@clemson.edu`. (Corresponding author: Ge Lv).

[2] J. Dean is with the Department of Rehabilitation Sciences, Medical University of South Carolina, Charleston, SC 29425, USA. `deaje@musc.edu`.

Digital Object Identifier (DOI): see top of this page.

the potential for designing a task-agnostic control paradigm by altering an individual's CM as it eliminates the need for joint-specific reference kinematics.

In this paper, we propose a CM shaping paradigm for lower-limb exoskeletons that provides task-agnostic assistance while preserving voluntary motion. Compared with prior work [20], which introduced the concept and showed simulation-level feasibility, this work makes three substantive advances: 1) a rigorous closed-loop analysis proving ultimate boundedness of both the nonlinear disturbance observer (NDO) estimation error and the CM tracking error with an exponentially decaying transient; 2) real-time implementation on a bilateral hip exoskeleton (Fig. 1); and 3) human-subject validation across multiple locomotor contexts, where the x-axis CM component is shaped in six non-disabled subjects during treadmill walking at different speeds and inclines, ground-stair transitions, and sit-to-stand tasks. The shaping law tracks the CM of a virtual reference model built from each user's real-time, self-selected gaits, eliminating the need to enforce pre-defined joint references. To explicitly account for human contribution, we further introduce an NDO that estimates human joint torques online and embeds them in the control law. Experimental results demonstrate effective modulation of muscular effort, with an average reduction of 22% with assistance and an average increase of 21% under resistance across both steady-state locomotion and task transitions, with a unified set of control parameters.

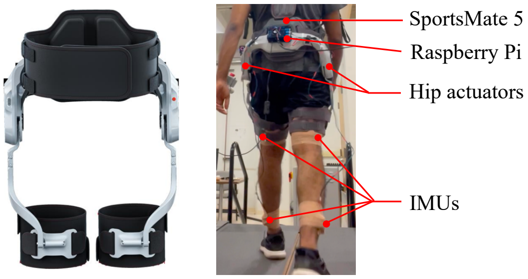

Fig. 1. The SportsMate 5 exoskeleton (left, Enhanced Power Technology Co., Ltd., Shenzhen, China) equipped with two highly backdrivable hip actuators, worn by a subject with externally mounted inertial measurement units (IMUs) and a Raspberry Pi (right).

The remainder of the paper is organized as follows. Sec. II presents the human-exoskeleton dynamics, CM shaping strategy, and NDO properties. Sec. III describes the bilateral hip exoskeleton and the reference-CM case study. Sec. IV details the experimental model and protocol. Sec. V reports the results, and Sec. VI concludes the paper.

II. DYNAMICS AND CONTROL DESIGN

This section models the human-exoskeleton system as a biped, presents a CM shaping strategy with a guaranteed control solution, and introduces a novel NDO for human joint torque estimation. The overall control structure is shown in Fig. 2, with each component detailed later.

A. Dynamics of the Human-Exoskeleton System

We model a human wearing an exoskeleton as one whole biped and express its Euler-Lagrange dynamics as [21]

$$M\ddot{q} + C\dot{q} + N + A^T\lambda = \tau, \tag{1}$$

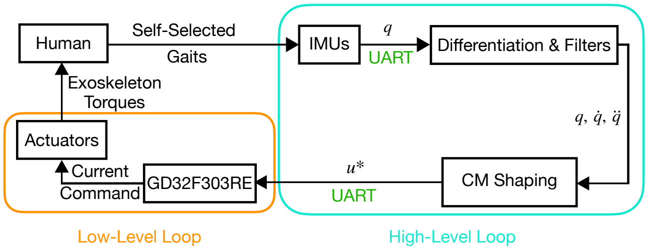

Fig. 2. Overall structure of the exoskeleton control system.

where $q = (\mathrm{x}, \mathrm{y}, \phi, q_s^T)^T \in \mathbb{R}^{\mathrm{n}}$ is the generalized coordinate vector, n is the number of degrees of freedom (DoFs), (x, y) are the Cartesian coordinates in the inertial reference frame (IRF), ϕ is the absolute angle with respect to the vertical axis, and q_s denotes relative joint angles. The matrix $M \in \mathbb{R}^{\mathrm{n}\times\mathrm{n}}$ is the positive definite inertia matrix, $C \in \mathbb{R}^{\mathrm{n}\times\mathrm{n}}$ is the Coriolis/centrifugal matrix, and $N \in \mathbb{R}^{\mathrm{n}}$ denotes the gravitational force vector. The constraint matrix A, defined as the gradient of holonomic constraint functions, maps the ground reaction force vector $\lambda = \hat{\lambda} + \check{\lambda}\tau$ into the overall dynamics, where $\hat{\lambda} = S(\dot{A}\dot{q} - AM^{-1}N)$, $S = (AM^{-1}A^T)^{-1}$, and $\check{\lambda} = SAM^{-1}$ [21]. All inertial parameters in these matrices combine the human and exoskeleton values, thus no separate detailed human neuromusculoskeletal model is needed. The overall torque τ sums up the human joint torque vector τ_{hum} and the exoskeleton torque vector $\tau_{\mathrm{exo}} = Bu$, where $B = (0_{\mathrm{p}\times(\mathrm{n}-\mathrm{p})}, I_{\mathrm{p}\times\mathrm{p}})^T \in \mathbb{R}^{\mathrm{n}\times\mathrm{p}}$ is the mapping matrix for exoskeleton torques from p actuators.

B. Centroidal Momentum of the Human-Exoskeleton System

For a multi-link biped, the velocity vector v_G of each biped link with respect to its body frame is given as

$$v_G = J_G\dot{q} \in \mathbb{R}^{6\mathrm{j}}, \quad J_G = [J_1^T, J_2^T, \cdots, J_{\mathrm{j}}^T]^T, \tag{2}$$

where $J_G \in \mathbb{R}^{6\mathrm{j}\times\mathrm{n}}$ is the system Jacobian matrix composed of body Jacobian matrices $J_i \in \mathbb{R}^{6\times\mathrm{n}}$, $i \in \{1, 2, \cdots, \mathrm{j}\}$ for all j links [21]. The body momentum vector $h_{\mathrm{body}} \in \mathbb{R}^{6\mathrm{j}}$ that contains the body momentum of each link is then given as

$$h_{\mathrm{body}} = I_G v_G, \quad I_G = \mathrm{diag}\{I_{G1}, I_{G2}, \cdots, I_{Gj}\}, \tag{3}$$

where $I_G \in \mathbb{R}^{6\mathrm{j}\times 6\mathrm{j}}$ is composed of inertia tensor matrices $I_{Gi} = \mathrm{diag}\{m_i \cdot I_{3\times3},\ I_i \cdot I_{3\times3}\} \in \mathbb{R}^{6\times6}$, $i \in \{1, 2, \cdots, \mathrm{j}\}$ with m_i and I_i being the mass and moment of inertia of the i-th link, respectively. Finally, we project h_{body} onto the biped's CoM by left-multiplying the adjoint transformation matrix $X_G \in \mathbb{R}^{6\mathrm{j}\times6}$ to obtain the CM as

$$h_G = X_G^T I_G J_G \dot{q} := A_G \dot{q}, \tag{4}$$

where $A_G = X_G^T I_G J_G \in \mathbb{R}^{6\times\mathrm{n}}$ is the CM matrix [18].

Remark 1: The CM in (4) contains both linear and angular momenta, each with three elements. If we assume the human ambulates in the sagittal plane (the $\mathrm{x} - o - \mathrm{y}$ plane in Fig. 5), the linear momentum along z axis and the angular momenta about x and y axes are zero, *i.e.*, A_G only contains three non-zero rows. Moreover, during each continuous phase of a gait cycle, h_G is differentiable with $\dot{h}_G = A_G\ddot{q} + \dot{A}_G\dot{q}$ [18].

C. Centroidal Momentum Shaping Controller Design

We now introduce the control strategy to alter a user's CM based on a reference profile. Given a differentiable reference h_G^{ref} and its time derivative $\dot{h}_G^{\text{ref}}$, we can track h_G^{ref} by satisfying the following relationship:

$$\dot{h}_G^{\text{ref}} - \dot{h}_G + K_p(h_G^{\text{ref}} - h_G) = 0, \tag{5}$$

where $K_p \in \mathbb{R}^{6\times 6}$ is a diagonal, positive definite matrix. This formulation drives $\dot{h}_G$ to follow $\dot{h}_G^{\text{ref}}$, while the proportional gain K_p reduces the error between h_G and h_G^{ref} (Fig. 3). Substituting $\dot{h}_G$ in (5) with $A_G\ddot{q} + \dot{A}_G\dot{q}$, we obtain

$$A_G\ddot{q} = \dot{h}_G^{\text{ref}} - \dot{A}_G\dot{q} + K_p(h_G^{\text{ref}} - A_G\dot{q}). \tag{6}$$

Substituting $\ddot{q}$ from (1) and plugging it into (6), we have

$$A_G M^{-1} B_\lambda u = H + \dot{h}_G^{\text{ref}} - \dot{A}_G\dot{q} + K_p(h_G^{\text{ref}} - A_G\dot{q}), \tag{7}$$

where $B_\lambda = B - A^T\check{\lambda}B$, $H = A_G M^{-1}(C\dot{q} + N + A^T\hat{\lambda}) - A_G M^{-1}(I - A^T\check{\lambda})\tau_{\text{hum}}$. Therefore, choosing u to satisfy (7) ensures the tracking behavior in (6).

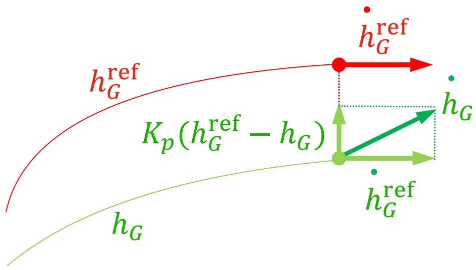

Fig. 3. Conceptual illustration of CM tracking via (5).

From Remark 1, the matrix A_G has only three non-zero rows for a sagittal-plane model, which simplifies (7) into three equivalent equations with u as the unknown. This implies that when an exoskeleton has more than three actuators in the sagittal plane, there are infinitely many solutions for the control law u. To specify one solution from these candidates, we employ an optimization procedure to determine u as

$$\begin{aligned} \min_{u} \quad & u^T W u \\ \text{s.t.} \quad & A_G M^{-1} B_\lambda u = g(q, \dot{q}), \\ & u_{\text{lower bound}} \le ||u||_2 \le u_{\text{upper bound}}, \end{aligned} \tag{8}$$

where $W \in \mathbb{R}^{\text{p}\times\text{p}}$ is a diagonal, positive semi-definite weight matrix that can be adjusted to tailor control allocation at specific joints, $g(q, \dot{q})$ denotes the right-hand side of (7). We select $u^T W u$ as the objective function to minimize torques exerted by exoskeleton actuators for a possible energy-efficient solution. Applying the Lagrange multiplier method [22], we can analytically solve (8) as:

$$\begin{aligned} u^* &= W^{-1}D^T(DW^{-1}D^T)^{-1}g(q, \dot{q}), \\ D &= A_G M^{-1} B_\lambda. \end{aligned} \tag{9}$$

Solving (8) and (9) requires knowledge of human joint torques τ_{hum}, whose estimation will be achieved via an NDO in Sec. II-D. Furthermore, because the proposed control strategy provides partial assistance for non-disabled users, they retain primary control of their gait stability.

D. Human Joint Torque Estimation via NDO

The proposed control strategy requires knowledge of human joint torques τ_{hum}, which can be challenging to measure directly in practice. To address this, we propose a novel NDO [23] to estimate a modified form of the human input $M^{-1}(I - A^T\check{\lambda})\tau_{\text{hum}}$ in (9) based on human joint kinematics. It is worth noting that we estimate this term instead of τ_{hum} directly to mitigate the effects of possible small eigenvalues from M.

Left multiplying M^{-1} on both sides of (1) yields

$$\ddot{q} + M^{-1}(C\dot{q} + N + A^T\hat{\lambda}) = M^{-1}B_\lambda u^* + z. \tag{10}$$

Here, $z = M^{-1}(I - A^T\check{\lambda})\tau_{\text{hum}}$ represents the "disturbance" term to be estimated. Equation (10) can be rewritten as

$$z = \ddot{q} + M^{-1}C\dot{q} + M^{-1}N + M^{-1}A^T\hat{\lambda} - M^{-1}B_\lambda u^*. \tag{11}$$

Defining $\hat{z}$ to be the estimate of z, we have:

$$\begin{aligned} \dot{\hat{z}} &= L(z - \hat{z}) \\ &= -L\hat{z} + L[\ddot{q} + M^{-1}(C\dot{q} + N + A^T\hat{\lambda} - B_\lambda u^*)], \end{aligned} \tag{12}$$

where $L \in \mathbb{R}^{\text{n}\times\text{n}}$ is a diagonal, positive definite matrix to be designed. In practice, we update $\hat{z}$ as $\hat{z}_{k+1} = \hat{z}_k + \Delta_t \cdot l(\hat{z}_k, q, \dot{q}, \ddot{q}, u^*)$, where Δ_t is the sampling period and $l(\cdot)$ denotes the right-hand side of (12) at the current state and input. The estimation error $e_N = z - \hat{z}$ is governed by

$$\dot{e}_N = \dot{z} - \dot{\hat{z}} = \dot{z} - Le_N. \tag{13}$$

Assuming that $\dot{z}$ is bounded, the estimation error e_N is uniformly ultimately bounded, as shown in the following theorem.

Theorem 1: For dynamics in (1), if $||\dot{z}||_2 \le \beta \in \mathbb{R}^+$ and $\theta \in (0, 1)$, then the estimation error e_N in (13) is uniformly ultimately bounded by $2\beta P_{\max}/(\theta Q_{\min})$, where $(\cdot)_{\min}$ and $(\cdot)_{\max}$ denote minimum and maximum eigenvalues, respectively, and P and Q satisfy the Lyapunov equation $PL + L^T P = Q$ [24].

Proof: Since L is positive definite, for any positive definite matrix Q, there exists a unique positive definite matrix P such that $PL + L^T P = Q$ (Theorem 4.6, [24]). Choosing $V(e_N) = e_N^T P e_N$ as a Lyapunov function, we have

$$\begin{aligned} \dot{V} &= \dot{e}_N^T P e_N + e_N^T P \dot{e}_N \\ &= (\dot{z} - Le_N)^T P e_N + e_N^T P(\dot{z} - Le_N) \\ &= 2\dot{z}^T P e_N - e_N^T Q e_N \\ &\le 2\dot{z}^T P e_N - Q_{\min}||e_N||^2. \end{aligned} \tag{14}$$

Assuming $\dot{z}$ is bounded by $\beta \in \mathbb{R}^+$, we have

$$\dot{z}^T P e_N \le ||\dot{z}|| \cdot ||Pe_N|| \le \beta ||Pe_N|| \le \beta P_{\max}||e_N||$$

for $\dot{z}^T P e_N$ in (14), therefore

$$\begin{aligned} \dot{V} &\le 2\beta P_{\max}||e_N|| - Q_{\min}||e_N||^2 \\ &= 2\beta P_{\max}||e_N|| - (1-\theta)Q_{\min}||e_N||^2 - \theta Q_{\min}||e_N||^2 \\ &\le -(1-\theta)Q_{\min}||e_N||^2, \ \forall ||e_N|| \ge 2\beta P_{\max}/(\theta Q_{\min}), \end{aligned}$$

where $\theta \in (0, 1)$. Therefore, with $\alpha_1(e_N) = \alpha_2(e_N) = e_N^T P e_N$ and $W_3(e_N) = (1-\theta)Q_{\min}||e_N||^2$, the estimation error is uniformly ultimately bounded by $2\beta P_{\max}/(\theta Q_{\min})$ (Theorem 4.18, [24]). ■

Remark 2: The assumption $\|\dot{z}\| \leq \beta$ for some $\beta \in \mathbb{R}^+$ can be verified numerically from experimental data and is not overly restrictive. Since $\dot{z}$ depends on joint angles, $\tilde{\tau}_{\text{hum}}$, and their time derivatives, and these quantities remain bounded during locomotion [25], assuming bounded $\|\dot{z}\|$ is reasonable.

Using the NDO-estimated $\hat{z}$, the closed-loop CM tracking error is uniformly ultimately bounded with an exponentially decaying transient, as formalized in the theorem below.

Theorem 2: For a differentiable reference h_G^{ref} and bounded e_N (Theorem 1), the control law (9) with the NDO estimate $\hat{z}$ ensures that the CM tracking error $e = h_G^{\text{ref}} - A_G\dot{q}$ is uniformly ultimately bounded by $\frac{\|A_G\|}{(K_p)_{\min}} \cdot \frac{2\beta P_{\max}}{\theta Q_{\min}}$. Moreover, e converges exponentially during each continuous phase.

Proof: Taking the time derivative of $e = h_G^{\text{ref}} - A_G\dot{q}$ yields

$$\dot{e} = \dot{h}_G^{\text{ref}} - \dot{A}_G\dot{q} - A_G\ddot{q}. \tag{15}$$

Substituting $\ddot{q}$ from (1) and $M^{-1}(I - A^T\check{\lambda})\tau_{\text{hum}}$ with z yields

$$\begin{aligned} A_G\ddot{q} =& A_G M^{-1}(-C\dot{q} - N - A^\top\lambda + \tau) \\ =& -A_G M^{-1}(C\dot{q} + N + A^\top\hat{\lambda} - B_\lambda u^*) + A_G z. \end{aligned} \tag{16}$$

Since u^* is the optimal solution of (8), replacing $A_G M^{-1}B_\lambda u^*$ with (7) and z with $\hat{z}$, we have

$$\begin{aligned} A_G\ddot{q} =& \cancel{-A_G M^{-1}(C\dot{q} + N + A^T\hat{\lambda})} + A_G z + \\ & [\cancel{(A_G M^{-1}(C\dot{q} + N + A^T\hat{\lambda})} - A_G\hat{z} + \dot{h}_G^{\text{ref}} - \dot{A}_G\dot{q} + \\ & K_p(h_G^{\text{ref}} - A_G\dot{q})] \\ =& A_G e_N + \dot{h}_G^{\text{ref}} - \dot{A}_G\dot{q} + K_p e. \end{aligned} \tag{17}$$

Plugging (17) into (15) yields

$$\begin{aligned} \dot{e} =& \cancel{\dot{h}_G^{\text{ref}}} - \xcancel{\dot{A}_G\dot{q}} - (A_G e_N + \cancel{\dot{h}_G^{\text{ref}}} - \xcancel{\dot{A}_G\dot{q}} + K_p e) \\ =& \ -K_p e - A_G e_N. \end{aligned} \tag{18}$$

Therefore, e follows an exponentially stable linear system driven by the NDO estimation error e_N. Solving for e yields

$$e = e^{-K_p t}e(0) - \int_0^t e^{-K_p(t-s)}A_G e_N(s)\,ds. \tag{19}$$

Therefore,

$$\begin{aligned} \|e\| \leq & \ e^{-(K_p)_{\min}\cdot t}\|e(0)\| \\ & + \int_0^t e^{-(K_p)_{\min}\cdot(t-s)}\|A_G\|\,\|e_N(s)\|\,ds. \end{aligned}$$

Since e_N is uniformly ultimately bounded by $2\beta P_{\max}/(\theta Q_{\min})$ (Theorem 1), $\exists\ T > 0$ such that for all $t \geq T$,

$$\begin{aligned} \|e\| \leq & e^{-(K_p)_{\min}\cdot(t-T)}\|e(T)\| \\ & + \frac{\|A_G\|}{(K_p)_{\min}} \cdot \frac{2\beta P_{\max}}{\theta Q_{\min}}\left(1 - e^{-(K_p)_{\min}\cdot(t-T)}\right), \end{aligned}$$

which implies

$$\limsup_{t\to\infty} \|e\| \leq \frac{\|A_G\|}{(K_p)_{\min}} \cdot \frac{2\beta P_{\max}}{\theta Q_{\min}}. \tag{20}$$

Therefore, e is uniformly ultimately bounded, and converges to a neighborhood of the origin exponentially fast between impacts within a gait cycle. ■

III. Bilateral Hip Exoskeleton System

We implemented the CM shaping controller in (9) on SportsMate 5, selected for the central role of hip musculature in gait propulsion [25], its low mass (3.2 kg) and high backdrivability to preserve voluntary motion. This section outlines the overall system architecture in Fig. 2.

A. *SportsMate 5 Exoskeleton*

SportsMate 5 is equipped with two brushless DC motors (ERMotor 5008). Each compact motor (50 × 18 mm) provides high torque density (21.4 Nm/kg), low rotor inertia (0.09 kg·cm^2), and overload capacity, delivering 7.5 Nm rated and 22.5 Nm peak torque. A quasi-direct-drive transmission (planetary gears and belt, 25:1) reduces damping and friction, yielding a backdrivability ratio of 78.4 and low backdrive torque (0.096 Nm) to support voluntary motion. Torque is regulated at 400 Hz using a GD32F303RE microprocessor (ARM Cortex-M4, 120 MHz, 512 kB ROM, 64 kB RAM), two 14-bit single-turn absolute magnetic encoders, and current sensors. All onboard electronics are powered by a 3200 mAh lithium battery. Bench-top tests (Table I, Fig. 4) showed reliable torque tracking: both actuators had sub-1 Nm RMSE and about 0.4 s settling time for 4 and 6 Nm steps, with gains above 0.91 for 2 Nm sinusoids across all tested frequencies.

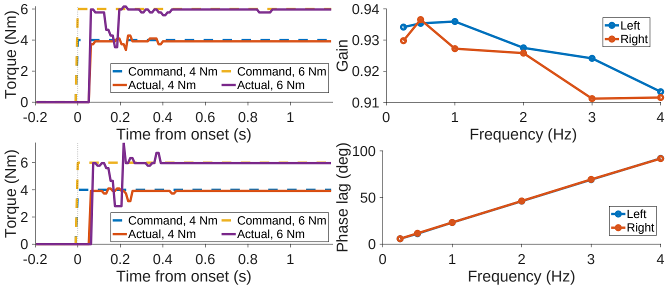

Fig. 4. Step responses (left) and sinusoidal torque tracking gain and phase lag (right) of SportsMate 5's actuators.

TABLE I

Bench-top characterization of SportsMate 5.

Side	Step RMSE (Nm)	Settling (ms)	Gain @1Hz	Lag @1Hz (°)	Gain @2Hz	Lag @2Hz (°)
Left	0.909	411.0	0.936	23.21	0.927	46.11
Right	0.975	426.3	0.927	23.25	0.926	46.26

B. *Human Kinematics Measurements*

We utilized IMUs (NGIMU, x-io Technologies Ltd., Bristol, UK) to measure human joint kinematics (Fig. 1, right) for the configuration vector of the experimental model (to be specified in Sec. IV-A). The IMUs applied manufacturer-provided onboard calibration to the raw inertial measurements and an Attitude and Heading Reference System fusion algorithm [26] to smooth the output data. For each subject, the IMUs were first initialized in the upright posture, and data collection began after the first 20 samples once signals stabilized. The angular information of human lower extremities was then transmitted to a Raspberry Pi 4B (8GB LPDDR4-3200 SDRAM, Cortex-A72 64-bit SoC, 1.8 GHz) via UART protocol. We computed numerical derivatives to determine the corresponding angular velocities and applied a moving average filter with a 71-sample window to reduce noise in the acceleration.

C. Control Architecture

The overall control architecture includes two loops: a high-level loop for computing u^* in (9) based on the IMU-measured joint kinematics and NDO-estimated human joint input in (12), and a low-level loop for its realization. We added a Raspberry Pi to interface with IMUs and compute the torque command in `C` at a real-time frequency of approximately 150 Hz (a similar frequency was achieved in [27]). The torque command is sent via UART to SportsMate 5's microprocessor, where the embedded ER-Driver regulates actuator current to track the desired torque (torque constant: 0.083 Nm/A). Although the Raspberry Pi controller can run at 550 Hz, we set the update rate to match SportsMate 5's communication frequency.

IV. EXPERIMENTAL STUDY

In this section, we introduce the experimental model, present a special case of reference CM design, and outline the associated experimental protocols and procedures.

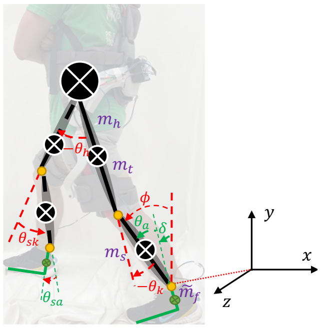

Fig. 5. Human-exoskeleton models for experimental implementation (4-DoF, red) and NDO evaluation (8-DoF, red + green).

A. Experimental Model

With two actuators designated to assist hip flexion/extension, SportsMate 5 is unlikely to have a direct impact on the ankle joints. We therefore adopted a 4-DoF point-feet biped model (Fig. 5) [28] to derive u^* for experiments given its reasonable fidelity in representing angular CM [29] and the computational capability of the onboard Raspberry Pi. Although SportsMate 5 applies torque only at the hips, the commanded exoskeleton torques are derived from a whole-body dynamic objective (i.e., the CM), rather than from joint-level pre-defined reference trajectories.

The model's generalized coordinates are given as $q_{\text{exp}} = (\phi, \theta_{\text{k}}, \theta_{\text{h}}, \theta_{\text{sk}})^T \in \mathbb{R}^4$ (Fig. 5, red), where k, h, and sk denote the stance knee, hip, and swing knee, respectively. Each subject's joint angles are measured in real time using four IMUs on both thighs and shanks, and the model is individualized using each subject's measured limb lengths and estimated inertial parameters from [30]. The experimental model is defined based on an IRF located at an individual's stance foot. To address the IRF changes during stance leg transitions, we employed two identical 4-DoF models anchored to each foot. During experiments, the model associated with the current stance leg was used to compute u^* and then sent to the ipsilateral hip actuator. We also assumed that the control command u^* was distributed equally between the two actuators with opposite signs, since left and right hip torques are approximately symmetric throughout the gait cycle [30]. To ensure safety, we saturated actuator torques to ±10 Nm. Since the 4-DoF model assumes no sliding of the stance foot, we can eliminate λ in (9) and thus $B_\lambda = B$ [28].

B. Case Study: Reference Centroidal Momentum Design

Tracking CM profiles based on pre-defined joint kinematics is incompatible with task-agnostic control. We propose to design a real-time reference CM as a case study that adapts dynamically to an individual's voluntary motion without constraining their gaits. In this case, we track the CM of a virtual reference model that has identical gaits to the individual, but with scaled limb inertial parameters, *i.e.*, its dynamics are given as

$$M_{\text{ref}}\ddot{q}_{\text{virtual}} + C_{\text{ref}}\dot{q} + N_{\text{ref}} + A^T\lambda_{\text{ref}} = \tau_{\text{hum}}, \tag{21}$$

where the configuration vector q and its time derivative $\dot{q}$ are the same as in (1), *i.e.*, identical kinematics to an individual's self-selected gait patterns. The matrices M_{ref}, C_{ref}, N_{ref}, and λ_{ref} in (21) are defined similarly to those in (1), but with scaled limb inertial parameters. Therefore, the reference CM is not a template shared across tasks. Instead, it is generated online from each user's real-time, self-selected motion with modified limb inertial parameters. Task agnosticism comes from applying one CM shaping framework across locomotor tasks, not from assuming similar CM trajectories. In this paper, we scale human mass and inertia via a parameter k_i, *i.e.*,

$$m_i^{\text{ref}} = k_i \cdot m_i, \quad I_i^{\text{ref}} = k_i \cdot I_i,$$

where $k_i > 0$ is the scaling factor. When $k_i > 1$, the exoskeleton produces torques to mimic a reference model heavier than the individual, and we define this mode as the resistive mode ("R"). Conversely, when $k_i < 1$, the exoskeleton is considered to be in assistive mode ("A") because the reference CM is defined based on reduced inertial parameters. Based on (21), its reference CM is given as

$$h_G^{\text{ref}} = A_G^{\text{ref}}\dot{q}, \qquad \dot{h}_G^{\text{ref}} = \dot{A}_G^{\text{ref}}\dot{q} + A_G^{\text{ref}}\ddot{q}_{\text{virtual}}, \tag{22}$$

where $\ddot{q}_{\text{virtual}}$ can be substituted from (21) as

$$\ddot{q}_{\text{virtual}} = M_{\text{ref}}^{-1}(-C_{\text{ref}}\dot{q} - N_{\text{ref}} - A^T\lambda_{\text{ref}} + \tau_{\text{hum}}). \tag{23}$$

Substituting the above h_G^{ref} and $\dot{h}_G^{\text{ref}}$ into $g(q, \dot{q})$ in (9) constructs the control law, which tracks the desired CM instead of joint-level kinematics. Combined with the exoskeleton's highly backdrivable actuation system, it should enhance flexibility for users when interacting with the exoskeleton. The desired CM can take forms other than scaled inertial parameters, and alternative definitions will be explored in future studies. Nevertheless, we observe benefits of the shaping strategy based on this particular reference CM in Sec. V.

C. Experiment Protocol

Overall, six non-disabled subjects (s1-s6, age: 25.7 ± 3.7, mass: 70.6 ± 11.3 kg, height: 1.76 ± 0.07 m) were recruited for the experiments, where a similar sample size is considered acceptable in other exoskeleton studies [31]. The experimental protocol was approved by the Institutional Review Board (IRB2022-0322), and subject consent was obtained prior to the start of all experiments. The subjects participated

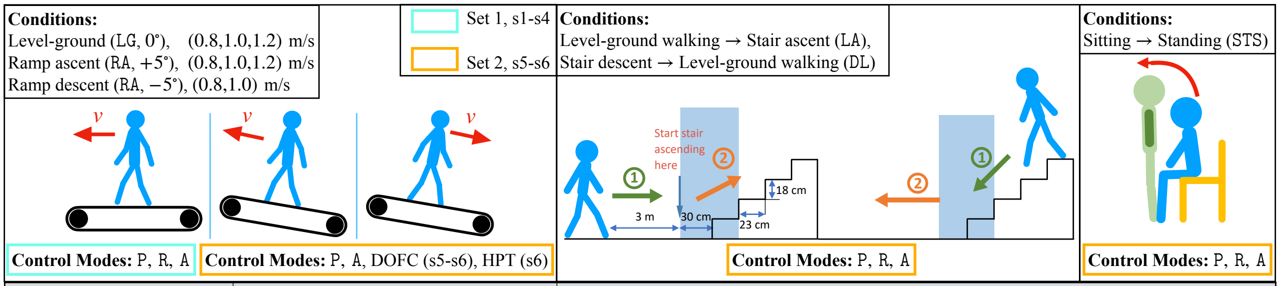

Control Modes	Characteristic	Intended Role
Passive (P)	$k_i = 1.00$	Exoskeleton worn, actuators off.
Resistive (R)	$k_i = 1.20$	Mimic the behavior of a heavier individual, harder to walk (more muscle demand).
Assistive (A)	$k_i = 0.85$	Mimic the behavior of a lighter individual, easier to walk (less muscle demand).

Fig. 6. Summary of experimental sets and the associated conditions.

in two sets of experiments wearing SportsMate 5, with the conditions and task acronyms summarized in Fig. 6. For comparison during treadmill walking, we implemented the Delayed Output Feedback Controller (DOFC, s5-s6) [32] and the Hip-Phase-Based Torque Profile Controller (HPT, s6) [5]. We selected DOFC as a representative task-agnostic hip-exoskeleton controller and complementary baseline to CM shaping. We included HPT as a secondary baseline because it is a representative kinematics-based adaptive torque controller using a reference torque profile. Key hardware and control differences among methods are summarized in Table II.

For all experiments, we set $K_p = 10 \cdot I_{6\times6}$ (pilot tuned) to produce comfortable hip torques, and $L = 100 \cdot I_{4\times4}$ in the NDO for rapid convergence to Winter's hip torque profile [30] in simulation [20]. We kept k_i fixed within the A and R modes to test whether unified parameters can provide task-agnostic assistance. Because SportsMate 5 has only two hip actuators, (9) can shape only one sagittal-plane CM component. We therefore shaped the x-axis linear component (walking direction), which contains most of the walking momentum [33]. From pilot tuning, k_i was set to 0.85 for A and 1.20 for R to provide beneficial torques without excessive magnitude.

TABLE II
COMPARISON OF CM SHAPING AND OTHER CONTROLLERS.

Controller	Platform	Inputs	Reference
CM shaping	SportsMate 5; 3.2 kg; 7.5/22.5 Nm	Kinematics + NDO	Real-time CM from user gait
DOFC [32]	GEMS; 2.1 kg; N/A/12 Nm	Hip angles	Delayed hip feedback
HPT [5]	e-Walk V1; 5 kg; 13/35 Nm	Hip angles + phase variable	Pre-defined phase-based torque profile

During experiments, subjects were not informed of the underlying control modes. All recorded data were segmented into gait cycles using heel strikes from two instrumented treadmill force plates (Set 1) or hip velocities from onboard IMUs (Set 2). We recorded EMG from Rectus Femoris (RF), Biceps Femoris (BF), and Gluteus Medius (GM) using Trigno Avanti sensors (Delsys Inc., MA, USA), where RF is a hip flexor, BF a hip extensor, and GM a primary hip abductor and secondary hip extensor [25]. EMG signals were bandpass filtered (20–500 Hz), rectified, and low-pass filtered at 6 Hz. They were then normalized to the maximum ensemble-average peak across repetitions and trials, yielding values as a percentage of peak filtered EMG.

V. RESULTS & DISCUSSION

We present estimated human joint torques, exoskeleton torques, EMG results, and CM in Figs. 7 to 11. In all figures, 0% of the gait cycle represents heel strike, while 100% represents the next heel strike of the same leg, and positive/negative torques denote hip extension/flexion, respectively.

A. Nonlinear Disturbance Observer

The estimated human hip torques using the proposed NDO are shown in Fig. 7. In the left panel, both the shape and magnitude of the estimated torques are comparable to those in Winter's dataset [30], indicating that the proposed NDO is sufficiently accurate to estimate τ_{hum} to compute u^*, even with the simplified 4-DoF model (Fig. 5, red). To further assess the NDO's performance, we used human joint kinematics from [34] to estimate hip torques based on an 8-DoF model (Fig. 5, red + green) and compared them with those from [34].

To further evaluate robustness to model mismatch, we added 10% parametric uncertainty into the estimation process for the 8-DoF model. Estimated hip torques remained close to the actual torques (Fig. 7, right), with small errors over most of the gait cycle. Spikes near 50% of the gait cycle coincide with stance-leg transition and the associated IRF change. For the 8-DoF model, RMSE ranged from 0.20 to 0.24 Nm/kg and R^2 ranged from 0.60 to 0.84, indicating reasonable performance comparable to existing methods [13].

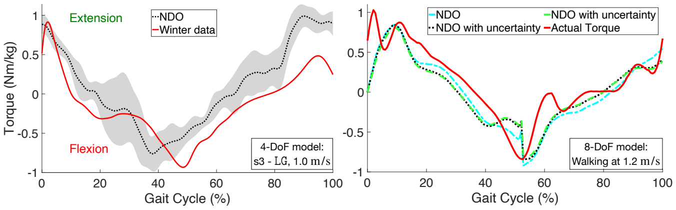

Fig. 7. Mean ± 1·SD of NDO-estimated hip torques: comparison with Winter's dataset (left) and dataset [34] under random parameter uncertainties (right).

B. Muscle Activities

Figs. 8 and 9 show ensemble-averaged EMG for Set 1 experiments (averaged over subjects and trials). Overall, A reduces muscle activation by offloading work, whereas R increases demand because users must overcome added resistance. The effect size varies with walking speed, since muscle force and work scale with speed [35]. Among the measured muscles, BF shows the largest change relative to P mode.

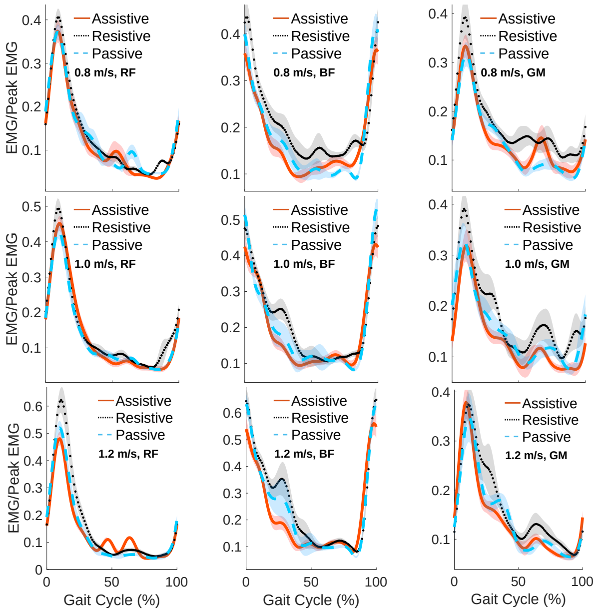

Fig. 8. Mean ± 1 · SD EMG averaged across incline conditions and subjects in Set 1 experiments.

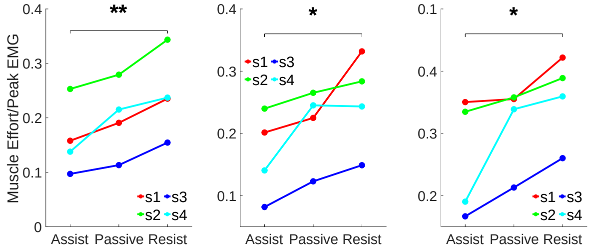

Fig. 9. Muscular effort (24) for s1-s4 at 0.8, 1.0, and 1.2 m/s (left to right). Statistical significance was tested with repeated-measures ANOVA; $*$ denotes $P < 0.05$ and $**$ denotes $P \leq 0.01$.

In `A` mode, assistive hip extension during stance (Fig. 10, left) reduces BF demand and lowers BF EMG [25]. BF activity also decreases in late swing because extension torque helps decelerate the leg and reduces braking demand. RF shows modest reductions in pre-swing and early swing, consistent with assistive flexion torque. In contrast, GM changes little across conditions because sagittal-plane assistance does not directly support its frontal-plane stabilization role as a hip abductor [25]. Overall, `A` selectively offloads targeted hip flexor/extensor muscles while preserving lateral-stability strategy, as indicated by similar GM patterns across `P`, `A`, and `R` modes.

In contrast, `R` mode generally increased muscle activation because users had to overcome added resistance. As shown in Fig. 8, both hip extensor and flexor EMG were higher in `R` than in `P`. During stance, resistive flexion torque opposed hip extension, increasing BF demand. This interpretation is consistent with Fig. 10 (right), where z-axis angular CM is lower in `R` than in `A` during treadmill walking, indicating slower leg motion under similar voluntary input. Results from other subjects and CM components are similar and are not presented.

C. Muscular Efforts

For each subject, muscle effort was first normalized to the maximum peak EMG value of each muscle across all trials,

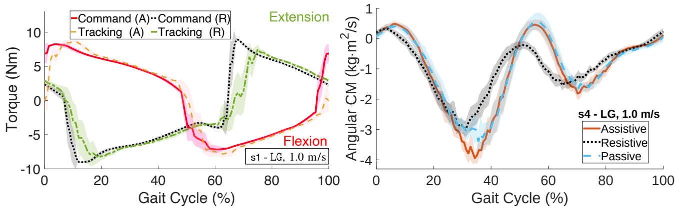

Fig. 10. Mean ± 0.5·SD of commanded vs. realized actuator torque (left) and z-axis angular CM (right) during `LG` at 1.0 m/s.

and then averaged across all muscles and trials over a full gait cycle to enable consistent comparison across subjects, *i.e.*,

$$\text{Muscle Effort} = \frac{1}{6}\frac{1}{n_{\text{cond}}}\sum_t\sum_i \frac{\text{iEMG}_{i,t}}{\text{EMG}_{\max,i}}, \qquad (24)$$

where n_{cond} is the number of trials within a walking condition, $\text{iEMG}_{i,t}$ is the integrated EMG of muscle i in trial t, $i \in \{\text{RF}_{\text{L,R}}, \text{BF}_{\text{L,R}}, \text{GM}_{\text{L,R}}\}$, and $\text{EMG}_{\max,i}$ denotes the maximum EMG value of muscle i across all trials. Note that the muscle efforts for `LA` and `DL` encompass the level-ground walking phase, the stair ascent/descent phase, and the transitions between these two phases, respectively. To further assess muscular effort across subjects, we computed the ensemble average, *i.e.*, the mean individual muscle efforts across subjects:

$$\text{Ensemble Effort} = \frac{1}{n_{\text{subject}}}\sum_k \text{Muscle Effort}_k, \qquad (25)$$

where n_{subject} is the number of subjects in Set 1 or 2, and $k \in \{s1, s2, s3, s4\}$ or $\{s5, s6\}$ depending on the task. In Fig. 11, for Set 1 experiments, `A`/`R` modes significantly reduced/increased muscle effort compared to the `P` mode, consistent with the observations in Sec. V-B. Quantitatively, `A` reduced ensemble-averaged muscle effort (25) by 19%, 22%, and 25% at 0.8, 1.0, and 1.2 m/s, respectively, whereas `R` mode increased effort by 22%, 20%, and 20% at the same speeds. Compared with DOFC, CM shaping achieved lower muscle effort across all walking conditions, with the largest gap at 1.2 m/s. This may be because DOFC tracks user motion less accurately at higher speeds, resulting in less timely assistive torques and higher muscular demand. Compared with HPT, CM shaping reduced muscle effort at 0.8 and 1.0 m/s and performed similarly at 1.2 m/s, indicating more consistent performance across walking conditions. During `LA` and `DL`, both `A` and `R` reduced effort, likely because the imposed torques provided stabilizing support and reduced balance-related co-contraction, similar to handrail assistance [36]. During `STS`, `A` reduced effort by 37%, whereas `R` increased it by 33% relative to `P`.

VI. CONCLUSION

This paper presented a task-agnostic CM shaping paradigm for hip exoskeleton assistance that does not prescribe joint trajectories. The controller tracks a virtual reference model defined based on each individual's gaits and integrates an NDO for real-time human torque estimation. We proved ultimate boundedness of the NDO estimation error and the closed-loop CM tracking error with an exponentially decaying transient. Experiments with six non-disabled subjects across treadmill walking (various speeds and inclinations), ground-stair transitions, and sit-to-stand showed consistent modulation

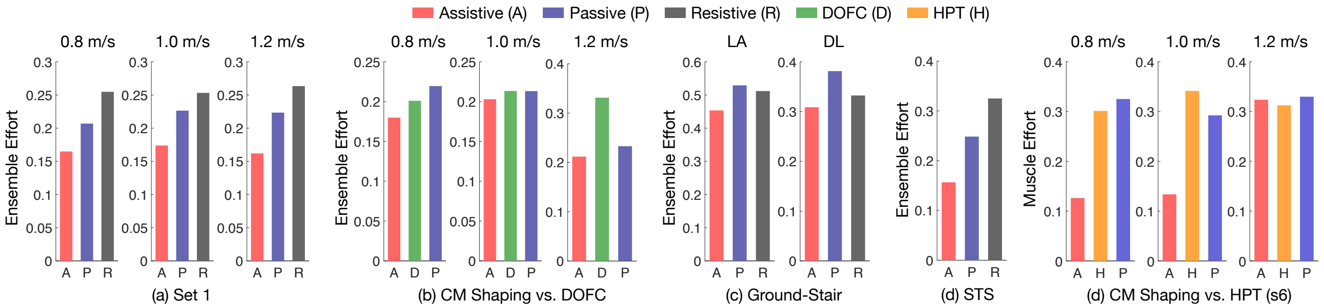

(a) Set 1 (b) CM Shaping vs. DOFC (c) Ground-Stair (d) STS (d) CM Shaping vs. HPT (s6)

Fig. 11. Muscular efforts comparison for Set 1 and Set 2 experiments.

of muscular effort, including an average 22% reduction in assistance mode and a 21% increase in resistance mode. These results demonstrate that CM shaping is a practical trajectory-free strategy for cross-task augmentation while preserving voluntary motion. Future work includes shaping additional CM components, customizing assistance through optimization, and validating performance in clinical populations.

REFERENCES

[1] R. Baud, A. R. Manzoori, A. Ijspeert, and M. Bouri, "Review of control strategies for lower-limb exoskeletons to assist gait," *J. NeuroEng. Rehabil.*, vol. 18, no. 1, pp. 1–34, 2021.

[2] T. Wang, Y. Zhu, T. Zheng, D. Sui, S. Zhao, and J. Zhao, "Palexo: A parallel actuated lower limb exoskeleton for high-load carrying," *IEEE Access*, vol. 8, pp. 67 250–67 262, 2020.

[3] L. M. Mooney, E. J. Rouse, and H. M. Herr, "Autonomous exoskeleton reduces metabolic cost of human walking during load carriage," *J. NeuroEng. Rehabil.*, vol. 11, no. 1, pp. 1–11, 2014.

[4] B. Johnson and M. Goldfarb, "A preliminary study on the feasibility of using a knee exoskeleton to reduce crouch gait in an adult with cerebral palsy," in *IEEE Int. Conf. Biomed. Robot. Biomechat.*, 2020, pp. 48–53.

[5] A. R. Manzoori, D. Malatesta, J. Primavesi, A. Ijspeert, and M. Bouri, "Evaluation of controllers for augmentative hip exoskeletons and their effects on metabolic cost of walking: explicit versus implicit synchronization," *Front. Bioeng. Biotechnol.*, vol. 12, p. 1324587, 2024.

[6] Y. Sun, Y. Tang, J. Zheng, D. Dong, X. Chen, and L. Bai, "From sensing to control of lower limb exoskeleton: A systematic review," *Annu. Rev. Control*, vol. 53, pp. 83–96, 2022.

[7] D. Sanz-Merodio, M. Cestari, J. C. Arevalo, and E. Garcia, "Control motion approach of a lower limb orthosis to reduce energy consumption," *Int. J. Adv. Robot. Syst.*, vol. 9, no. 6, p. 232, 2012.

[8] M. K. Shepherd and E. J. Rouse, "Design and validation of a torque-controllable knee exoskeleton for sit-to-stand assistance," *IEEE/ASME Trans. Mechatron.*, vol. 22, no. 4, pp. 1695–1704, 2017.

[9] W. Ma, H. Cheng, R. Huang, and Q. Chen, "Gait planning with dynamic movement primitives for lower limb exoskeleton walking upstairs," in *IEEE Int. Conf. Robot. Biomim*, Dec. 2018, pp. 703–708.

[10] S. Wang, L. Wang, C. Meijneke, E. Van Asseldonk, T. Hoellinger, G. Cheron, Y. Ivanenko, V. La Scaleia, F. Sylos-Labini, M. Molinari *et al.*, "Design and control of the mindwalker exoskeleton," *IEEE Trans. Neural Syst. Rehabil. Eng.*, vol. 23, no. 2, pp. 277–286, 2014.

[11] Y. Chen, S. Miao, G. Chen, J. Ye, C. Fu, B. Liang, S. Song, and X. Li, "Learning to assist different wearers in multitasks: efficient and individualized human-in-the-loop adaptation framework for lower-limb exoskeleton," *IEEE Trans. Robot.*, vol. 40, pp. 4699–4718, 2024.

[12] M. Ding, M. Nagashima, S.-G. Cho, J. Takamatsu, and T. Ogasawara, "Control of walking assist exoskeleton with time-delay based on the prediction of plantar force," *IEEE Access*, vol. 8, pp. 138 642–138 651, 2020.

[13] D. D. Molinaro, K. L. Scherpereel, E. B. Schonhaut, G. Evangelopoulos, M. K. Shepherd, and A. J. Young, "Task-agnostic exoskeleton control via biological joint moment estimation," *Nature*, vol. 635, no. 8038, pp. 337–344, 2024.

[14] N. J. Cronin, "Using deep neural networks for kinematic analysis: Challenges and opportunities," *J. Biomech.*, vol. 123, p. 110460, 2021.

[15] G. Lv, H. Zhu, and R. D. Gregg, "On the design and control of highly backdrivable lower-limb exoskeletons: A discussion of past and ongoing work," *IEEE Control Syst. Mag.*, vol. 38, no. 6, pp. 88–113, 2018.

[16] J. Lin, N. V. Divekar, G. Lv, and R. D. Gregg, "Optimal task-invariant energetic control for a knee-ankle exoskeleton," *IEEE Control Syst. Lett.*, vol. 5, no. 5, pp. 1711–1716, 2020.

[17] J. Lin, R. D. Gregg, and P. B. Shull, "Improving task-agnostic energy shaping control of powered exoskeletons with task/gait classification," *IEEE Rob. Autom. Lett.*, vol. 9, no. 8, pp. 6848–6855, 2024.

[18] D. E. Orin, A. Goswami, and S.-H. Lee, "Centroidal dynamics of a humanoid robot," *Auton. Robots*, vol. 35, no. 2, pp. 161–176, 2013.

[19] C. Bayon, A. Emmens, M. Afschrift, T. Van Wouwe, A. Keemink, H. Van Der Kooij, and E. Van Asseldonk, "Can momentum-based control predict human balance recovery strategies?" *IEEE Trans. Neural Syst. Rehabil. Eng.*, vol. 28, no. 9, pp. 2015–2024, 2020.

[20] M. Yu and G. Lv, "Task-invariant centroidal momentum shaping for lower-limb exoskeletons," *IEEE Conf. Decis. Cont.*, pp. 2054–2060, 2022.

[21] R. M. Murray, Z. Li, and S. S. Sastry, *A mathematical introduction to robotic manipulation*. NW Boca Raton, FL: CRC Press, 2017.

[22] R. T. Rockafellar, "Lagrange multipliers and optimality," *SIAM Rev.*, vol. 35, no. 2, pp. 183–238, 1993.

[23] W.-H. Chen, D. J. Ballance, P. J. Gawthrop, and J. O'Reilly, "A nonlinear disturbance observer for robotic manipulators," *IEEE Trans. Ind. Electron.*, vol. 47, no. 4, pp. 932–938, 2000.

[24] H. K. Khalil, *Nonlinear Systems; 3rd ed.* Upper Saddle River, NJ: Prentice-Hall, 2002.

[25] J. Perry and J. Burnfield, *Gait analysis: normal and pathological function*. CRC Press, 2024.

[26] S. Madgwick, "An efficient orientation filter for inertial and inertial/magnetic sensor arrays," *Report x-io and University of Bristol (UK)*, vol. 25, pp. 113–118, 2010.

[27] P. R. Shetty, J. A. Menezes, S. Song, A. J. Young, and M. K. Shepherd, "Ankle exoskeleton control via data-driven gait estimation for walking, running, and inclines," *IEEE Robot. Autom. Lett.*, vol. 10, no. 6, pp. 5855–5862, 2025.

[28] E. R. Westervelt, J. W. Grizzle, C. Chevallereau, J. H. Choi, and B. Morris, *Feedback Control of Dynamic Bipedal Robot Locomotion*. NW Boca Raton, FL: CRC Press, 2018.

[29] N. Hale, M. Yu, R. Gurchiek, and G. Lv, "Whole-body angular momentum estimation using reduced-order models," in *Annu. Int. Conf. IEEE Eng. Med. Biol. Soc.* IEEE, 2026, to appear.

[30] D. A. Winter, *Biomechanics and Motor Control of Human Movement*. Hoboken: John Wiley & Sons, 2009.

[31] Q. Zhang, V. Nalam, X. Tu, M. Li, J. Si, M. D. Lewek, and H. H. Huang, "Imposing healthy hip motion pattern and range by exoskeleton control for individualized assistance," *IEEE Robot. Autom. Lett.*, vol. 7, no. 4, pp. 11 126–11 133, 2022.

[32] B. Lim, J. Lee, J. Jang, K. Kim, Y. J. Park, K. Seo, and Y. Shim, "Delayed output feedback control for gait assistance with a robotic hip exoskeleton," *IEEE Trans. Robot.*, vol. 35, no. 4, pp. 1055–1062, 2019.

[33] G. C. Simoneau and D. E. Krebs, "Whole-body momentum during gait: a preliminary study of non-fallers and frequent fallers," *J. Appl. Biomech.*, vol. 16, no. 1, pp. 1–13, 2000.

[34] E. Reznick, K. R. Embry, R. Neuman, E. Bolívar-Nieto, N. P. Fey, and R. D. Gregg, "Lower-limb kinematics and kinetics during continuously varying human locomotion," *Sci. Data*, vol. 8, no. 1, p. 282, 2021.

[35] A. Hof, H. Elzinga, W. Grimmius, and J. Halbertsma, "Speed dependence of averaged emg profiles in walking," *Gait & Posture*, vol. 16, no. 1, pp. 78–86, 2002.

[36] T. IJmker, C. Lamoth, H. Houdijk, M. Tolsma, L. Van Der Woude, A. Daffertshofer, and P. Beek, "Effects of handrail hold and light touch on energetics, step parameters, and neuromuscular activity during walking after stroke," *J. NeuroEng. Rehabil.*, vol. 12, no. 1, p. 70, 2015.